The shadow function method in aureole scattering

N.V. Kustova and A.G. Borovoi

Institute of Atmospheric Optics,
Siberian Branch of the Russian Academy of Sciences, Tomsk

Received April 14, 2006

New effective method called the shadow function method has been worked out for the problems of light scattering by large, as compared to the wavelength, nonspherical particles. As against the standard Fraunhofer diffraction patterns, the shadow functions have a number of important advantages, which make their computation easier. Numerical values of shadow functions for hexagonal crystals of cirrus clouds are presented. These data are of interest for both aureole measurements in clouds and lidar sensing of cirrus clouds.

Introduction

The small-angle scattering method, which in atmospheric optics is called the aureole scattering, is one of the most promising in optics of light-scattering media. The experimentally measured scattering phase function theoretically can be a source of information on shape and size distribution of particles. However today, when interpreting experimental data, the authors would have to assume a spherical shape of particles,[1–4] because the theory of small-angle scattering by nonspherical particles is insufficiently advanced. The purposes of this paper are the further development of the theory and its application to the cirrus-cloud optics.

The small-angle scattering is understood as formation of a specific component in a scattered field only for relatively large, as compared to wavelengths, particles (i.e., $\lambda \ll d$, where λ is the wavelength and d is the characteristic particle size) regardless of the refractive index. This component is formed due to the Fraunhofer diffraction of an incident wave by a particle shade line and, hence, it is essential in a narrow cone of scattering directions of $\theta \approx \lambda/d$ relative to the direction of the incident wave propagation.

In general, in the problem of light scattering by large ($\lambda \ll d$) particles of random shapes, the scattered field consists of two components, which are suitable to be called refracted and shadow-forming fields.[5] The refracted field just near the particle surface is described by the geometrical optics approximation as the ensemble of beams reflected or refracted inside the particle. The shadow-forming field near the particle is a plane-parallel beam, propagating in the direction of the incident plane wave, which in its cross section corresponds to the particle projection and has an amplitude equal to the amplitude of the negatively signed incident field. A superposition of the refracted and shadow-forming fields results in their elimination, i.e., in a shadow. When propagating further from the particle, both fields are transformed in accordance with the wave equations. In particular, the shadow-forming field in the wave zone (i.e., at the distances $R \gg d^2/\lambda$) is described by the above mentioned plane wave Fraunhofer diffraction by the particle shade line.

As a rule, the shadow-forming field inside the Fraunhofer diffraction cone ($\theta \approx \lambda/d$) significantly exceeds the refracted one in amplitude; hence, the latter can be easily neglected, but it can essentially contribute into the cone $\theta \approx \lambda/d$ for crystals with parallel edges. Actually, the crystal parallel edges at some orientations of the particle are equivalent to a plane-parallel plate. Such edges form plane-parallel light beams coming out from the crystal in the direction of the incident wave propagation as well. Such beams will be called transmitted as opposite to the above-described shadow-forming beams. Thus, small-angle scattering for crystals with parallel edges will be determined by the Fraunhofer diffraction of both the shadow-forming and transmitted beams.

The state-of-the-art of the computer techniques allows one to easily calculate the diffraction pattern for a shadow-forming beam of a random cross form and, hence, to find the small-angle scattering phase function at a given orientation of a randomly-shaped particle. However, of particular interest in practice are the scattering phase functions averaged over a random spatial orientation of particles. Besides, cirrus ice crystals are predominantly oriented in a horizontal plane while keeping random azimuth orientation. The computation of mean small-angle scattering phase functions is compute-intensive because of a large dynamic range of intensity values in diffraction patterns.[6–8] Therefore, the shape of the particle shadow is usually substituted for approximately a circle,[9,10] rectangle, or spheroid.[11,12] Such substitution is justified in direct problems of light scattering, but is impossible in inverse ones, where shapes of particles are to be restored from the experimentally measured scattering phase functions.

In this work we consider the problem of small-angle scattering by randomly oriented particles independently of the shape of shadow or transmitted beams. To overcome the above-mentioned

0235-6880/06/10 778-06 $02.00

computational problem, we go to the Fourier transform of the scattering phase function, which further will be called the shadow function. Note, that in our previous work[13] this function was called S-function. As compared to the scattering phase function, the shadow function has a number of advantages. First, it has an evident geometric meaning, which allows a visual estimation of calculation results. Second, the function is strongly zero outside a finite domain, the size of which is equal to the maximal diameter of the particle shadow. Third, the shadow function, in contrast to the small-angle scattering phase function, is a smooth function with a small dynamic range of values. And fourth, the function is wavelength-independent, because it is determined by the scattered field of the near particle zone.

1. Shadow function for the shadow-forming beam

The shadow-forming beam, propagating in the direction of the incident plane wave propagation immediately behind the particle, is described by the equation

$$\eta(\boldsymbol{\rho}) = \begin{cases} 1 & \text{inside the particle's shadow (projection)}, \\ 0 & \text{out of the shadow}, \end{cases} \quad (1)$$

where $\boldsymbol{\rho} = (x, y)$ are the coordinates on the plane normal to the plane wave incidence direction; the function $\eta(\boldsymbol{\rho})$ will be called the shadow indicator. At large distances from the particle, i.e., inside the wave zone, this field is transformed into a diverging spherical wave, where the field distribution over scattering directions is defined by the so-called scattering amplitude $f(\mathbf{n})$, which for the shadow-forming field is described by the classical Fraunhofer diffraction formula:

$$f(\mathbf{n}) = \frac{k}{2\pi i} \int \eta(\boldsymbol{\rho}) \exp(-ik\mathbf{n}\boldsymbol{\rho}) \mathrm{d}\boldsymbol{\rho}, \quad (2)$$

where $\mathbf{n}$ is the projection of the scattering direction $\boldsymbol{\Omega}$ ($|\boldsymbol{\Omega}| = 1$) to the plane (x, y); $k = 2\pi/\lambda$. The small-angle scattered field essentially differs from zero only near the forward scattering direction at $|\mathbf{n}| \ll 1$, therefore, the scattering amplitude (2) can be formally considered as a function defined on the unlimited plane of $\mathbf{n}$ values. Then the energy conservation law is reduced to the Parseval theorem and has the following simple form:

$$\int |f(\mathbf{n})|^2 \, \mathrm{d}\mathbf{n} = \int \eta^2(\boldsymbol{\rho}) \mathrm{d}\boldsymbol{\rho} = s, \quad (3)$$

where s is the area of the particle shadow.

The small-angle scattering amplitude $f(\mathbf{n})$ contains full information on the shadow indicator $\eta(\boldsymbol{\rho})$, which can be retrieved from the experimentally measured scattering amplitude by the trivial 2-D Fourier transform. However, in optics, instead of the complex scattering amplitude $f(\mathbf{n})$, the real quadratic value of the field

$$I(\mathbf{n}) = |f(\mathbf{n})|^2 \quad (4)$$

is commonly measured in experiments.

The real function $I(\mathbf{n})$ is a standard Fraunhofer diffraction pattern from a slit in a $\eta(\boldsymbol{\rho})$-shape black screen. In terms of the light scattering theory, $I(\mathbf{n})$ corresponds to the conventional scattering phase function $p(\mathbf{n})$, differing only, as is evident from Eq. (3), by the normalization factor

$$p(\mathbf{n}) = I(\mathbf{n}) / s. \quad (5)$$

There arises a question whether or not all information on a shadow shape is retained in the scattering phase function? The answer follows from the Fourier transform of the phase function or, which is more convenient, the diffraction pattern $I(\mathbf{n})$:

$$S(\boldsymbol{\rho}) = \int I(\mathbf{n}) \exp(ik\mathbf{n}\boldsymbol{\rho}) \mathrm{d}\mathbf{n}, \quad (6)$$

where the inverse Fourier transform brings us back to the initial diffraction pattern

$$I(\mathbf{n}) = \left(\frac{k}{2\pi}\right)^2 \int S(\boldsymbol{\rho}) \exp(-ik\mathbf{n}\boldsymbol{\rho}) \mathrm{d}\boldsymbol{\rho}. \quad (7)$$

Substituting Eqs. (2) and (4) into Eq. (6), we obtain the following equation:

$$S(\boldsymbol{\rho}) = \int \eta(\boldsymbol{\rho}') \eta(\boldsymbol{\rho}' - \boldsymbol{\rho}) \mathrm{d}\boldsymbol{\rho}', \quad (8)$$

which has a clear geometrical meaning of the shadow indicator autocorrelation. Just this function we will call the shadow function. Thus, if to measure experimentally the scattering phase function instead of the scattering amplitude, we can retrieve not the initial shadow indicator, but only a smoother autocorrelation or shadow function.

Enumerate main properties of the shadow function (8). First, it takes its maximal value in the center $\boldsymbol{\rho} = 0$; and the maximum is equal to the shadow area

$$S(0) = s. \quad (9)$$

Then, it quickly decreases, vanishing at a distance from the center equal to the shadow diameter in the given direction on the plane $\boldsymbol{\rho}$. If the shadow shape is convex, then the shadow function falls down monotonically in any direction. At $\boldsymbol{\rho} = 0$ it has a singularity in the form of a sharp peak. Here the directional derivative jumps with the sign reversion since $S(\boldsymbol{\rho}) = S(-\boldsymbol{\rho})$. The integral of the shadow function over the plane is equal to the squared shadow area

$$\int S(\boldsymbol{\rho}) \mathrm{d}\boldsymbol{\rho} = s^2. \quad (10)$$

Let us compare properties of scattering phase functions with those of shadow functions. A small-angle scattering phase function is formally defined by Eqs. (2)–(5) on unlimited plane of $\mathbf{n}$ values. Although it essentially differs from zero only in the central spot of $|\mathbf{n}| \le \lambda/d$ in size, there are also side diffraction lobes rapidly decreasing in magnitude and carrying an additional information on a shadow shape. Therefore, the choice of a certain limited area on $\mathbf{n}$, where the phase function is calculated, and cell sizes is always accompanied by difficulties. Moreover, the choice depends on the wavelength, which needs to be fixed in calculations. None of the above-mentioned problems appear in numerical calculations of shadow functions.

Moreover, note that the scattering phase function for nonspherical particles is quite complicated and oscillating function of two variables. Therefore, a particle of a complex shape is usually approximated by some simpler particle, mostly, a sphere. At a level of scattering phase functions, numerical fitting of phase function parameters for different particle shapes is a formal and unobvious procedure. One more advantage of shadow functions as compared to scattering phase functions is the fact that in this case the substitution of one particle shape to another, having a simpler shape or a superposition of shapes is a geometrically descriptive and physically justified procedure.

The above-introduced functions $\eta(\boldsymbol{\rho})$ and $S(\boldsymbol{\rho})$ depend on absolute sizes and shapes of particles. It is convenient for us to exclude the trivial dependence on absolute sizes and to consider only the dependence on particle shapes. To do this, we go from the dimensional variable $\boldsymbol{\rho}$ to dimensionless one $\mathbf{R}$ defined as

$$\boldsymbol{\rho} = \mathbf{R}\sqrt{s}, \tag{11}$$

where $\mathrm{d}\boldsymbol{\rho} = \mathrm{d}x\mathrm{d}y = s\mathrm{d}\mathbf{R}$.

The shadow indicator, written in these variables,

$$\eta_0(\mathbf{R}) = \eta(\boldsymbol{\rho}/\sqrt{s}), \tag{12}$$

will be called the reduced shadow indicator. Since $\eta_0(\mathbf{R})$ separates a unit area on the plane $\mathbf{R}$, just the reduced shadow indicator $\eta_0(\mathbf{R})$ characterizes the particle shape. Absolute sizes can be easily introduced through going to the variable $\boldsymbol{\rho}$. The autocorrelation (8) of the shadow indicator (12) gives the reduced shadow function

$$S_0(\mathbf{R}) = \int \eta_0(\mathbf{R}')\eta_0(\mathbf{R}' - \mathbf{R})\mathrm{d}\mathbf{R}' = S\left(\boldsymbol{\rho}/\sqrt{s}\right)/s, \tag{13}$$

which is defined only by a shadow shape and has the following properties:

$$S_0(0) = 1; \tag{14}$$

$$\int S_0(\mathbf{R})\mathrm{d}\mathbf{R} = 1. \tag{15}$$

In optics of scattering media, usual subject of study is not a single particle but a statistical ensemble of particles of some size, shape, and spatial orientation. In this case the detector summarizes all diffraction patterns (4) formed by different particles. If N is the number of particles, then the detector measures $N\langle I(\mathbf{n})\rangle$, where $\langle I(\mathbf{n})\rangle$ is the averaged-over-the-ensemble diffraction pattern of a single particle with the following properties:

$$\int \langle I(\mathbf{n})\rangle \mathrm{d}\mathbf{n} = \langle s\rangle; \tag{16}$$

$$\langle I(0)\rangle = \langle s^2\rangle/\lambda^2, \tag{17}$$

where $\langle s\rangle$ and $\langle s^2\rangle$ are the mean area and the mean squared area of the shadow. The Fourier transform (6) of the diffraction pattern $\langle I(\mathbf{n})\rangle$ gives the shadow function

$$\langle S(\boldsymbol{\rho})\rangle = \int \langle I(\mathbf{n})\rangle \exp(ik\mathbf{n}\boldsymbol{\rho})\mathrm{d}\mathbf{n} = \int \langle \eta(\boldsymbol{\rho}')\eta(\boldsymbol{\rho}' - \boldsymbol{\rho})\rangle \mathrm{d}\boldsymbol{\rho}' \tag{18}$$

with the properties

$$\langle S(0)\rangle = \langle s\rangle; \tag{19}$$

$$\int \langle S(\boldsymbol{\rho})\rangle \mathrm{d}\boldsymbol{\rho} = \langle s^2\rangle. \tag{20}$$

To exclude absolute sizes of particles, define the given shadow function for a statistical ensemble through Eq. (13), where the shadow area is changed to the mean area

$$S_0(\mathbf{R}) = \langle S\left(\boldsymbol{\rho}/\sqrt{\langle s\rangle}\right)\rangle / \langle s\rangle. \tag{21}$$

The normalizing condition (14) for this reduced function holds, while the condition (15) is substituted for the equation

$$\int S_0(\mathbf{R})\mathrm{d}\mathbf{R} = \langle s^2\rangle / \langle s\rangle^2. \tag{22}$$

1.1. Horizontally oriented particles

In a number of cases, ice cirrus crystals can have predominantly horizontal spatial orientation, in particular, ice plates are horizontally oriented with a probable spread of deviations from the horizon not more than 5°. The principal axes of ice columns are also in a horizontal plane at a comparatively random azimuth angle orientation. In this case, if one of the pairs of side faces is also horizontally oriented, such columns are called Parry-oriented. Note, that a number of halos, well known in atmospheric optics, are formed just by the horizontally oriented ice crystals.

Consider the simplest case of light normally incident on a hexahedral Parry-oriented column. Its shadow indicator (1) is a rectangle, the side ratio Q = length/width of which

$$Q = \text{altitude}/\text{diameter} \tag{23}$$

is commonly used in literature to describe hexagonal columns and plates. Here the diameter corresponds to

hexagonal sides and the altitude is the distance between hexagonal sides. At random azimuth orientation of such a column, the shadow function is to be averaged over the azimuth angle, that results in the one-variable function $S_0(r)$, where r is the distance from the center $\mathbf{R} = 0$.

Figure 1 shows the shadow functions (21) calculated at different values of Q; evidently, the circle function, shown in Fig. 1 for comparison, is the limiting one for them.

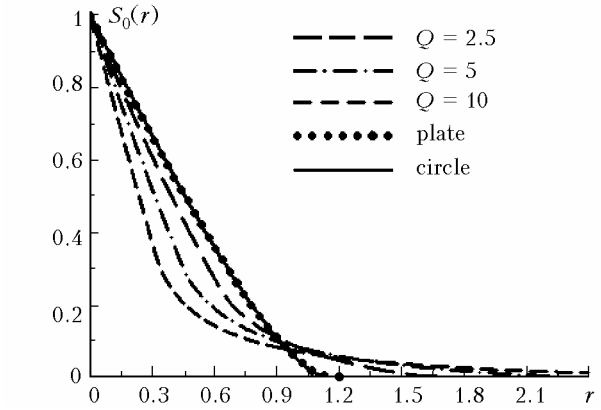

Fig. 1. Shadow functions for horizontally oriented hexagonal crystals.

The more elongated is the column, the more the shadow function deviates from the circle function. As is seen from Fig. 1, the shadow function for a horizontally oriented hexagonal plate only slightly differs from the circle function. Note that since the particle shadow area remains constant at such statistical averaging, all functions in Fig. 1 satisfy Eqs. (14) and (15).

1.2. Randomly oriented particles

In case of random orientation of particles in a three-dimensional space, areas of their projections change together with orientation and the reduced shadow functions satisfy Eq. (22). Values of integral parameter Q of shadow functions calculated for hexagonal columns and plates are given in Fig. 2.

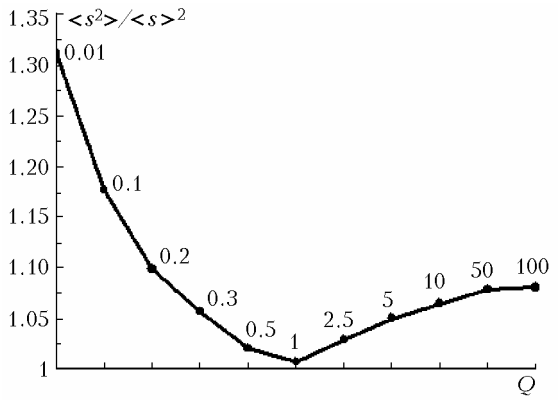

Fig. 2. Relative dispersion of shadow area for randomly oriented hexagonal columns and plates.

As is seen from Fig. 2, the cube-like form of crystals ($Q \approx 1$) is the extremum. Here the particle shape is the closest to sphere and, hence, the parameter $\mu = \langle s^2\rangle/\langle s\rangle^2$ little differs from unit. When going to plates ($Q < 1$), μ increases tending to the limiting value for a thin plate $\mu_1 = 4/3$, which is easy to obtain theoretically. When going to elongated columns ($Q > 1$), μ increases, but its limiting value $\mu_2 \approx 1.08$, which can be calculated analytically as well.

Shadow functions of randomly oriented hexagonal crystals are given in Fig. 3. Note the qualitative difference between columns and plates in shapes of shadow functions. As is seen from Fig. 3*a*, the shadow functions of hexagonal plates are close to the shadow function of a circle up to $r \approx 0.6$. The exceed above the circle shadow function arising at $1.6 > r > 0.6$ fills a narrow gap between the circle and the limiting for a thin plate shadow functions at decreasing Q. Note that this excess answers to the increase of the above-indicated μ value.

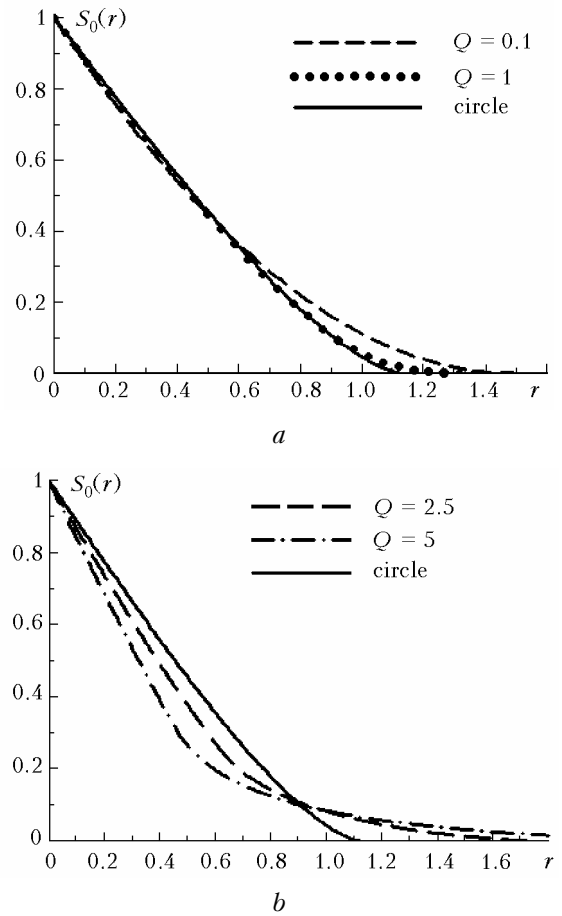

Fig. 3. Shadow functions for randomly oriented hexagonal crystals: plates (*a*) and columns (*b*).

For hexagonal columns at $Q \gg 1$ μ is not large. Therefore, a change in the shadow function shape with Q increase causes first (at $r \le 1$) a decrease of

$S_0(r)$ values as compared to the circle shadow function and then (at $r > 1$) the $S_0(r)$ excess above it (Fig. 3*b*).

Underline that at a level of shadow functions the substitution of particle shapes by simpler ones, in particular, by sphere, becomes a descriptive and physically justified procedure.

2. Shadow functions for transmitted beams

In case of shadow-forming beams the polarization of the electromagnetic wave can be neglected, because polarizations of incident and shadow-forming waves at small scattering angles are virtually the same. In the case of a crystal with parallel edges, the electromagnetic scattered field, propagating forward immediately behind the particle, consists of shadow-forming and transmitted beams. In this case polarizations in the transmitted beams differ essentially. Therefore, such fields are to be described with accounting for the polarization, i.e., as transverse vector fields:

$$\mathbf{E}(\rho) = -\mathbf{E}^0\eta_0(\rho) + \sum_{m=1}^{n}\mathbf{E}^m\eta_m(\rho). \qquad (24)$$

Here the first summand corresponds to the shadow-forming beam; n is the number of transmitted beams at a given particle orientation; $\mathbf{E}^0$ is the complex amplitude of an incident plane wave, and $\mathbf{E}^m$ are the corresponding amplitudes for the transmitted beams; $\eta_{0,m}$ are the indicator shape functions of shadow-forming and transmitted beams. The electromagnetic field, scattered at small angles in the particle wave zone, is defined through the vector scattering amplitude by the equation similar to Eq. (2):

$$\mathbf{F}(\mathbf{n}) = \frac{k}{2\pi i}\int\mathbf{E}(\rho)\exp(-ik\mathbf{n}\rho)\mathrm{d}\rho. \qquad (25)$$

In general, either quadratic field values $E_iE_j^*$ $(i, j = 1, 2)$ or their linear combination in the form of Stokes parameters $I_l (l = 1, 2, 3, 4)$ are the measurable variables in optics. Correspondingly, small-angle scattering at a level of quadratic field values is defined by the autocorrelation of the field (24) similarly to Eqs. (7) and (8). This autocorrelation is the direct generalization of the shadow function and has the following form:

$$A_{ij}(\rho) = \sum_{m=0}^{n}E_i^mE_j^{*m}S_m(\rho) + \sum_{\substack{m,t=o\\ m\neq t}}^{n}E_i^mE_j^{*t}S_{mt}(\rho). \qquad (26)$$

Here the first summand includes the autocorrelation for each beam while the second one – the cross terms describing the interference between the beams. Let us consider particles in the statistical ensemble as sufficiently large in size, so that at a single pass of the particle, the additional (related to the refractive index) phase incursion in the electromagnetic wave exceed 2π, i.e. $2\pi l + \varphi$, where l is integer and φ is the random variable equidistributed in the interval $[0, 2\pi]$. In this case, when averaging over the ensemble, the interference term in Eq. (26) can be neglected. Then only the first term remains of interest for the further consideration.

In the first summand of Eq. (26), the S_m functions are defined via the shape indicators of each beam η_m according to Eq. (8). Though the shadow notion is inapplicable to the transmitted beams, we will by analogy call the functions S_m shadow functions for transmitted beams. Thus, the calculation of the field autocorrelation $\langle A_{ij}(\rho)\rangle$ is reduced to calculation of autocorrelations of shadow-forming and transmitted beams. In this case, every beam is described by both the scalar shadow function $S_m(\rho)$ and the weighting coefficient $E_i^mE_j^{*m}$. In particular, the mean shadow function for the radiation intensity $I_1 = |\mathbf{E}|^2 = |E_1|^2 + |E_2|^2$ can be written as

$$\langle S(\rho)\rangle = \langle S^{\mathrm{sh}}(\rho)\rangle + \langle\sum_{m=1}^{n}|\mathbf{E}^m|^2\,S_m(\rho)\rangle =$$

$$= \langle S^{\mathrm{sh}}(\rho)\rangle + \langle S^{\mathrm{tr}}(\rho)\rangle. \qquad (27)$$

Remind that the two-dimensional Fourier transform of the shadow function (27) gives a statistically averaged diffraction pattern if to detect it with the use of a photoreceiver without a polarizer. In Eq. (27), the first summand corresponds to the shadow function of a shadow-forming beam while the second one is the shadow function of the transmitted beams. The inequality $\langle S^{\mathrm{tr}}(\rho)\rangle \le \langle S^{\mathrm{sh}}(\rho)\rangle$ follows from the energy conservation law. At $\rho = 0$ the relation $\langle S^{\mathrm{tr}}(0)\rangle = \sigma_{\mathrm{tr}}$ has a simple physical meaning of the mean scattering cross section for transmitted beams, and $\langle S^{\mathrm{sh}}(0)\rangle = \langle s\rangle$ for the shadow-forming ones. It is convenient to normalize the shadow function of transmitted beams by the same Eq. (21) as for the shadow-forming beam. Then the reduced function in the center $\mathbf{R} = 0$ is equal to the ratio $S_0^{\mathrm{tr}}(0) = \sigma_{\mathrm{tr}}/\langle s\rangle$. Further, as $r = |\mathbf{R}|$ increases, the reduced function of transmitted beams $S_0^{\mathrm{tr}}(\mathbf{R})$ decreases being less than the reduced function $\langle S_0^{\mathrm{sh}}(\mathbf{R})\rangle$ and remaining within the limits of its non-zero values.

The calculated shadow functions of the transmitted beams for randomly oriented hexagonal plates and columns at the refractive index equal to 1.31 are shown in Fig. 4.

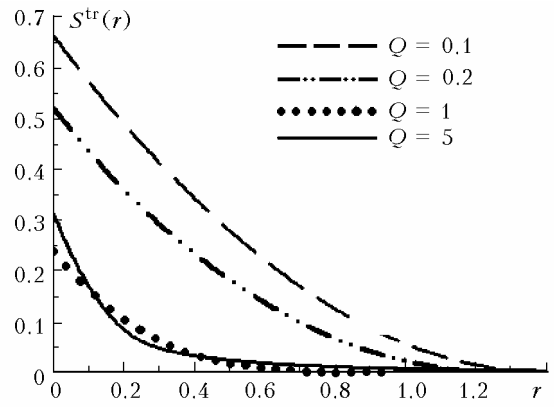

Fig. 4. Shadow functions of transmitted beams for randomly oriented hexagonal ice crystals.

As is seen, the scattering cross section of transmitted beams for plates attains 70% in comparison with the mean particle projection area <*s*>, while it does not exceed 30% for columns. Note that in atmospheric optics the accounting for the contribution of transmitted beams into the small-angle scattering is of practical importance for interpretation of aureole measurement data and lidar signals reflected from cirrus clouds.

Conclusion

The small-angle scattering by large, as compared to wavelengths, particles of irregular form is studied insufficiently to date. Published works cite either illustrative calculation results for a diffraction pattern obtained for a specific particle shape or attempts to approximate such a pattern by diffraction pattern of a circle with some effective radius. The shadow functions introduced in our work have a number of important advantages as compared to direct calculations of diffraction patterns and, hence, are effectively applicable in different problems of the small-angle scattering. The procedure of substituting a particle shape to a simpler one becomes physically justified and illustrative. The obtained estimates for the scattering cross section of the transmitted beams are of practical importance for problems of aureole scattering and laser sensing of cirrus clouds.

Acknowledgments

This work was financially supported by the Russian Foundation for Basic Research (Grants Nos. 05–05–39014 and 06–05–65141).

References

1. A.A. Isakov, Izv. Ros. Akad. Nauk, Ser. Fiz. Atmos. Okeana **30**, No. 2, 241–245 (1994).
2. A.A. Isakov, Atmos. Oceanic Opt. **10**, No. 7, 447–454 (1997).
3. A.A. Isakov, Atmos. Oceanic Opt. **11**, No. 12, 1117–1122 (1998).
4. P.P. Anikin and M.A. Sviridenkov, Izv. Ros. Akad. Nauk, Ser. Fiz. Atmos. Okeana **34**, No. 3, 390–394 (1998).
5. A.G. Borovoi, in: *Light Scattering Reviews*, ed. by A. Kokhanovsky (Springer-Praxis, Chichester, 2006), pp. 181–252.
6. Q. Cai and K.N. Liou, Appl. Opt. **21**, No. 19, 3569–3580 (1982).
7. Y. Takano and S. Asano, J. Meteorol. Soc. Jap. **61**, No. 2, 289–300 (1983).
8. A. Macke, J. Mueller, and E. Raschke, J. Atmos. Sci. **53**, No. 19, 2813–2825 (1996).
9. K. Muinonen, K. Lumme, J. Peltoniemi, and W.M. Irvine, Appl. Opt. **28**, No. 15, 3051–3060 (1989).
10. A. Macke, Appl. Opt. **32**, No. 15, 2780–2788 (1993).
11. A.G. Petrushin, Izv. Ros. Akad. Nauk, Ser. Fiz. Atmos. Okeana **23**, No. 5, 546–548 (1987).
12. A.G. Petrushin, Izv. Ros. Akad. Nauk, Ser. Fiz. Atmos. Okeana **30**, No. 3, 309–318 (1994).
13. A. Borovoi, E. Naats, U. Oppel, and I. Grishin, Appl. Opt. **39**, No. 12, 1989–1997 (2000).